HHS Public Access

Author manuscript

Magn Reson Med. Author manuscript; available in PMC 2017 February 01.

Published in final edited form as:

Magn Reson Med. 2016 February ; 75(2): 897–905. doi:10.1002/mrm.25655.

Flexible, 31 channel breast coil for enhanced parallel imaging performance at 3T

Ileana Hancu, PhD[1], **Eric Fiveland, MS**[1], **Keith Park, BS**[1], **Randy O. Giaquinto, AAS**[2], **Kenneth Rohling, AAS**[1], and **Florian Wiesinger, PhD**[3]

[1]GE Global Research Center, Niskayuna, NY, USA

[2]Correct Coil LLC, Cincinnati, OH, USA

[3]GE Global Research, Munich, Germany

Abstract

Purpose—To design, build and characterize the performance of a novel 3T, 31 channel breast coil.

Methods—A flexible breast coil, accommodating all breast sizes while preserving close to unity filling factors in all configurations, was designed and built. Its performance was compared to the performance of the current state-of-the-art, 16 channel breast coil (Sentinelle coil, Hologic, Bedford, MA, USA), in phantoms and *in vivo*.

Results—Better axilla coverage and lower inter-coil coupling (12% vs. 26%, as characterized by the average off-diagonal elements of the noise correlation matrix) was exhibited by our 31 channel coil compared to the 16 channel coil. Breast area SNR increases of 68% (phantom) and 28 ± 31% (*in vivo*) were demonstrated in the 3 volunteers studied when the 31 channel coil was used. For the 31 channel/16 channel arrays, respectively, two dimensional acceleration factors of L/R × S/I = 4.3 × 2.4 resulted in average g-factors of 1.10/1.68 (*in vitro*) and 1.28/2.75 (*in vivo*); acceleration factors of L/R × A/P = 3.0 × 2.8 resulted in average g-factors of 1.06/1.54 (*in vitro*) and 1.05/1.12 (*in vivo*).

Conclusion—A high performance breast coil was built; its capabilities were demonstrated in phantom and normal volunteer imaging experiments.

Keywords

breast; flexible; coil; MRI; cancer; 3T

Introduction

MRI of the breast is used increasingly frequently in the clinic, to screen high risk women (1), identify extent of disease prior to surgery (2), and on a more experimental basis, to monitor cancer treatment (3). The signal to noise ratio (SNR) and acceleration capability of

Corresponding author: Ileana Hancu, GE Global Research Center, One Research Circle, K1-NMR133, Niskayuna, NY 12309, hancu@ge.com, tel: 518-387-4703, fax: 518-387-6923.

current commercial breast coils can limit the diagnostic power of breast MRI exams, even if performed at 3T. For example, higher SNR and higher acceleration capability can be traded for higher temporal resolution of dynamic contrast enhanced (DCE) images, allowing better kinetic data modeling, and increased cancer detection specificity (4). Similarly, higher acceleration capability enables shorter echo time and readout duration for echo-planar based diffusion weighted imaging (DWI), reducing image distortion and blurring, and resulting in an improved image quality of DWI acquisitions (5).

While increasing the channel count of an array is a straightforward approach to increase image SNR or acceleration capability, the choice of array geometry for the breast anatomy is difficult. Since breast sizes in the wide population vary between 125 and 1900 ml (6), an array that has the the highest number of coils and the highest filling factor (i.e. the fraction of the coil volume occupied by the sample) for each coil in each individual subject is usually not an option. While multiple cup systems can be a good choice in a research environment (7), such approach is not commercially viable, due to the high cost incurred to build these multiple options. Commercial breast coil design has traditionally made the choice between lower channel count (up to 8 channels), rigid setups, that give good image uniformity, but comparatively low SNR, and the more dense arrays (up to 16 channels), that use coils mounted on movable plates (such as the Sentinelle breast coils (Hologic, Bedford, MA, USA)). This latter option enables good filling factors for the upper-most coils in all subjects, and works very well in women with large breasts. Yet for subjects with small breasts, only a few of the coils are relevant for imaging the desired anatomy; significantly, no coil exists in the anterior aspect of the breast, therefore reducing the achievable SNR in this configuration.

In this work, the design and implementation of a 3T, flexible breast array, capable to accommodate a large range of subjects without any hardware changes, is documented. The tuning/matching of this coil in phantoms simulating the entire range of human breast sizes and compositions is analyzed. A comparison between the performance of this coil and the 16 channel, Sentinelle coil, in phantoms and *in vivo* is also presented.

Methods

1. Flexible coil design

The 31 coils, of approximately square shape and 9 cm on a side, were arranged in 3 rows along the superior/inferior (S/I) direction, with 10/11/10 coils on each row, and printed on DuPont Pyralux™ AP 9252R flexible circuit material, using 5mm wide, 2 oz/ft^2 Cu traces (Figure 1a). The size of the coils was determined by the desired field of view in the S/I direction (21 cm) and by the need to allow coverage for the largest breasts, while maintaining axilla coverage for these extreme cases. The overlaps between coils were initially determined experimentally by printing single coils, and changing the overlaps (on an “average breast” curved geometry) until the mutual inductance between coils was minimized. Once printed on the circuit board, no degree of flexibility existed for changing the overlaps. The total number of coils was dictated by symmetry reasons, leading to 31, and not 32 coils. All major electrical components on the two “flaps” of the coil (tuning capacitors, diodes, baluns, inductors) were placed on the side of the circuit board away from the patient, along superior to inferior (S/I) direction and covered by 8 ribs; Figure 1a also

displays the 2 outermost ribs of the coil. Note that these ribs are not part of the structural support of the coil; they simply insure that no bending happens in the regions of the circuit board that contain most of the electronic components. The remaining, 7 central coils had their components facing towards the patient, and were covered by a rigid plastic section. In this implementation, the sheet has large flexibility to mold to different breast sizes, but no bending capability along the orthogonal, S/I direction. Figure 1b presents a cutout of the coil, displaying how the electrical structure fits within the mechanical structure. Note that the coil has 4 main mechanical parts: the (pink) main structure, the (yellow) sternum support, the (grey) sternum cover, and the (blue) interchangeable insert, which allows for maximum comfort for different body sizes.

The cables from each coil are routed transversally (right to left), through the middle of its corresponding row, through notches existent on the outside of ribs; they then enter the sternum area and are routed longitudinally (S/I) towards the abdominal region, where preamplifiers are located. Figure 1c shows an illustration of the view from underneath the coil, demonstrating the 6 bundles of cables being routed towards the abdominal region.

Figures 1d and 1e show top/side pictures of the coil (taken at the time the coil was completed and ready for patient use). All the mechanical parts of the coil (main patient support structure, support sternum section, sternum cover, removable top insert and the eight ribs), were 3D printed out of polycarbonate material. The patient side was covered with 1.25 cm vinyl coated foam (blue cover of Figure 1e), a standard MR patient positioning product that can be sponge cleaned.

Each of the coils has a circuit depicted in Figure 2. The baluns were spiral, self-shielded, of 18/4 mm diameter/thickness respectively, having 7000 Ω blocking impedance and 0.12 dB insertion loss at 128 MHz. The λ/2 cables were needed to extract the signals to the abdominal location, where the preamplifiers could be conveniently located. The additional two λ/4 lumped elements were added for preamplifier protection (note the diodes to ground in the schematics). The overlaps between neighboring coils were adjusted to minimize their mutual inductance. The tuning and matching procedure was iterative; each of the elements was first tuned and matched, while all the other elements were inactive. For the ensuing iterations, all elements were activated, and capacitor values were adjusted to bring elements back to the tuned and matched condition in the presence of the coupling of each element with its neighbors.

A multi-compartment torso phantom, shown in Figure 3a, was designed and 3D-printed for tuning this coil. Each "breast" had 3 independent compartments, and the "torso" was also split in a superior, middle and inferior compartment. This middle breast/torso compartments of this phantom represents an average torso and average breast phantom (500 ml each). The phantom was placed on the table with its handles down, enabling one to mold the flexible circuit board (connected to the sternum plastic section) in a repeatable tuning position, with the electronic components facing the person tuning the coil. When tuning, the middle breast/torso compartments of this phantom were filled with distilled water, using 1g/l $CuS0_4$ and 2.2g/l NaCl, simulating an average body load.

2. Network analyzer measurements

To characterize this coil on the bench, S11 and S21 measurements were performed on a HP 4395A network analyzer (Hewlett-Packard, Palo Alto, CA, USA), using the tuning phantom of Figure 3a. While all 31 S11 measurements were performed, only a limited number of S21 measurements were completed. More precisely, three randomized S21 measurements were done for each of the 31 coils of the array, out of which one was with a nearest neighbor, one with a next-nearest neighbor, and the third one with a random other coil in the array.

In order to understand how the tuning and matching of each coil changes as a function of breast size and composition, a second phantom setup was used (Figure 3b). A large elliptical torso phantom (of 26 and 41 cm diameters) filled with 1g/l $CuSO_4$ and 2.2 g/l NaCl dissolved in distilled water was used in conjunction with nine different spherical phantoms as breasts. These three sets of three identical phantoms (volumes of 225, 525 and 1700ml, respectively) were filled with water, 1.1 g/L CuSO4 and 0, 1.1 and 2.2g/l NaCl respectively. The sizes and salt concentrations of these phantoms are representative of sizes and breast compositions in a population of subjects, with 2.2g/l approximating an entirely dense breast, and 1.1g/l approximating a 50% fat containing breast (8)). The array was adjusted to mold to the size of each “breast set”, simulating the *in-vivo* situation. The tuning/matching of the coil elements were analyzed as a function of phantom.

3. Imaging studies

The purpose of these studies was to characterize the performance of our 31 channel array, and compare it to the performance of the state of the art, 16 channel Sentinelle coil. While the layout of the latter coil is not, known, it is likely that it contains 4 elements on each of the lateral paddles, while 8 elements are located on the central, sternum support. Both coils accommodate breast volumes of ~19 cm (S/I) by ~11.5 cm (R/L) by ~12.5 cm (A/P).

The phantom and *in vivo* scans were performed on a Discovery 3.0 T MR750w scanner (GE Healthcare, Waukesha, WI, USA), using both the 16/31 channel arrays. Transmit field homogeneity was optimized using the MultiDrive feature, which allows automated and independent adjustment of the RF pulse amplitude and phase control of the two birdcage transmit modes. Subjects gave informed consent before the study, which was conducted with the approval of the Institutional Human Research Review Committee.

A. In vitro experiments—To characterize coil performance *in vitro*, the torso phantom of Figure 3b, coupled to two 850 ml half sphere phantoms (@1.1g/l NaCl) was first scanned using the following four acquisitions

- **A.1.** 3D SPGR, TE/TR=1.7/3.7ms, Excitation=ON, using the 16 channel/31 channel arrays
- **A.2.** 3D SPGR, TE/TR=1.7/3.7ms, Excitation=ON, using the body coil for reception
- **A.3.** 3D SPGR, TE/TR=1.7/3.7ms, Excitation=OFF, using the 16 channel/31 channel arrays
- **A.4.** B_1^+ map, TE/TR=23/3150ms, Excitation=ON, using the body coil for reception

As neither the Sentinelle, nor the 31 channel coil was tuned using this particular phantom, this setup presents a fair challenge to both coils. While the torso of this phantom may be larger than the one of an average subject, its half-sphere breasts are similar to the ones of an average subject; it is unlikely for either of the 2 arrays to be more off-tune or off-match than they would be for a random patient (whose breast sizes can vary between 125ml and 1.9l (6), and can be 100% fatty or 100% dense). All four series used identical slice locations/coverage, with a field of view (FOV) of 48 cm, a 3mm slice thickness and an in plane resolution of 1.9 mm. The B_1^+ mapping relied on a spin echo based Bloch Siegert sequence (11).

B. In vivo experiments—To characterize the performance of the coils *in vivo*, after obtaining informed consent, three normal volunteers (bra sizes A-C) underwent a series of scans, as detailed below:

- **B.1.** 3D SPGR, TE/TR=1.7/3.7ms, Excitation=ON, acceleration factor=1, in plane resolution of 256x256, for a total of 44, 3mm thick slices (acquisition time 0:47min), using the 16/31 channel arrays
- **B.2** 3D SPGR, TE/TR=1.7/3.7ms, Excitation=ON, acceleration factor=1, in plane resolution of 256x256, for a total of 44, 3mm thick slices (acquisition time 0:47min), using the body coil for reception
- **B.3.** 3D SPGR, TE/TR=1.7/3.7ms, Excitation=OFF, acceleration factor=1, in plane resolution of 256x256, for a total of 44, 3mm thick slices (acquisition time 0:47min), using the 16/31 channel arrays
- **B.4.** Fat-suppressed 3D SPGR, TE/TR=2.1/4.4ms, Excitation=ON, acceleration factor=3 (R/L), in plane resolution of 340x240, for a total of 264, 1mm thick slices (acquisition time 0:49min).

The acquisitions used a FOV between 36 and 38 cm, using an axial orientation. The first three scans were performed to characterize coil performance *in vivo*. The last scan was a typical clinical acquisition, used for pre- and post-contrast DCE-MRI.

4. SNR and g-factor measurements

The performance of the 16 channel Sentinelle coil and the 31 channel coil was assessed in terms of SNR and parallel imaging g-factor (9,10) in a phantom and three healthy volunteers. For this purpose, receiver noise covariance/correlation information was derived from dedicated noise scans with the RF excitation turned off (protocols A.3 and B.3 described in the previous section). Coil sensitivities were measured differently *in vitro* and *in vivo*: Based on the uniform material properties of the phantom, *in vitro* coil sensitivities were determined by dividing the single coil images (protocol A.1) by the corresponding B_1^+ map (protocol A.4). For the *in vivo* case, coil sensitivities were obtained by dividing single coil images (protocol B.1) and body coil images (protocol B.2) of identical acquisition parameters. In both cases, masking was applied based on the body coil acquisition, using a threshold value obtained from the corresponding image histogram (i.e. first minimum in the histogram right to the noise peak). For the relative SNR comparison in the phantom, rigid image registration was used to align the two datasets. Because of highly non-rigid breast

positioning/displacement, this was not possible *in vivo*. Instead approximately corresponding slice locations were chosen manually. All processing was performed using Matlab (Mathworks, Natick, MA, USA).

Results

Table 1 displays the minimum, average and maximum S11 and S21 measurements, expressed in dB, for the 3 rows of 10, 11 and 10 coils respectively, taken on the phantom on which the array was tuned (Figure 3a). Note the relative uniformity of the S11 measurements—apart from a slightly lower performance of the superior row of coils. That is mostly due to the fact that three of the coils on that row had to be slightly detuned at the end of the tuning process, as they were slightly disturbing the transmit field. The uniformly low values of the S21 measurements confirm the limited coupling existent in the array.

This low coupling is also confirmed by Figure 4, which displays the receiver noise covariance matrix (left) and correlation matrix (right) for the 16 channel array (top) and the 31 channel array (bottom), using a "hot" color map. As usual, the elements of the correlation matrix are equal the same elements of the covariance matrix normalized by the corresponding diagonal element (12). Each of the four quadrants of Figure 4 shows the noise characteristics for the phantom setup (left) and one of the volunteers (right). The off-diagonal elements of the noise correlation matrix under in-vivo loading conditions are much smaller for the 31 channel array (12.3±12.0% ranging from 0.1 to 55.0%) than for the Sentinelle array (26.2±20.9% ranging from 1.3 to 80.5%), confirming the lower coupling existent in the 31 channel array. Note also the similarity between the noise correlation coefficients obtained in the phantom and in vivo, indicating loading independent SNR and parallel imaging performance.

Table 2 displays the S11 parameters for 5 of the coils on the central row, starting from the center (Ch 1) and heading to the outermost coil (Ch 5), as the spherical "breasts" of the Figure 3b phantom dramatically changed size and composition. The central channel, which "saw" the same torso phantom, irrespective of the "breasts", was omitted from this table. Note that these measurements were not taken on the phantom on which the array was tuned, hence they are overall lower than in the ideal case (displayed in Table 1). While an ideal coil will have S11 values less than −20dbB, and loading factors ($Q_{unloaded}/Q_{loaded}$) in excess of 10, indicating a sample dominated noise regime (13), it is common for high density arrays to fall short of this requirement (14). The advantage of a copper-dominated loss situation (and relative insensitivity to the sample), in which our coil is close to operating, is the fact that the array should perform similarly, irrespective of its loading/subject to be imaged. The two sets of outliers in Table 2 (Channel 4 with medium "breasts" and Channel 5 with large "breasts") correspond to a non-physical situation, in which the coil under investigation sees the large void between the end of the sphere and the beginning of the torso. The real anatomy allows for closer molding of the coil to the subject undergoing the exam, in particular since multiple-size inserts (Figure 1b) can be used to bring the coil close to the anatomy.

Figure 5 shows the un-accelerated SNR maps for the 16 channel Sentinelle array (left column) and the 31 channel coil (middle column). The two sets of images are displayed on the same scale. The relative SNR improvement in percentage ($100*(SNR_{31ch}-SNR_{16ch})/SNR_{16ch}$) is shown in the right hand column of Figure 5, using a linear color scale ranging from −50% to +150% (with the background at 0% appearing red). The top row of Figure 5 displays the middle axial slice; the bottom row shows the coronal plane passing through the middle of the "breasts". Note that significantly higher SNR can be achieved with the 31 channel coil in the axilla and sternum regions (which see up to 150% signal increases), as well as in the medial and anterior chest regions. In fact, it is only the most lateral regions of the breast that show up to 18% lower performance of the 31 channel coil compared to the Sentinelle coil. Due to the rigid geometry of the phantom, and the large size of the "torso", the setup was scanned without the blue insert (Figure 1b), which allowed the coil to be farther from the object than ideal. While this situation will not be encountered in vivo (as the patient will simply not have enough support), it highlights the need of using an adequately sized insert, to insure patient comfort, and to obtain the highest possible SNR. The relative SNR improvement over the two half-sphere breasts was found to be 68% (±40%), covering a range between −18% and 218%.

Figure 6 compares parallel imaging performance, quantified in terms of the g-factor, for the 16 channel Sentinelle coil and the 31channel array, in a phantom (left) and in one of the volunteers (right). The data was acquired fully sampled in a 3D acquisition (see the Methdos section), then artificially undersampled. The top three rows show coronal slices for 1D and 2D acceleration factors of L/R × S/I = 1.0 × 2.4, 4.3 × 1.0, and 4.3 × 2.4; whereas the bottom three rows show axial slices for acceleration factors of L/R × A/P = 1.0 × 2.8, 3.0 × 1.0, 3.0 × 2.8. The g-factor statistics (average and maximum), computed over the slices displayed in Figure 6 (breast area only for the axial scans) are summarized in Table 3. The 31 channel coil shows consistently low g-factors (*in vivo* and *in vitro*), and generally outperforms the 16 channel array, allowing for 1D and 2D acceleration with minimal SNR penalties (see, e.g. rows 3 and 6 of Table 3). Only for L/R acceleration does the 31 channel array appear slightly inferior. The results of Table 3 also confirm that the parallel imaging performance of the 31 channel coil is independent of its load; the *in vivo* results, acquired with a FOV of 36 cm, in a cup A volunteer, are similar with the phantom results, acquired with an imaging FOV of 48 cm, with half-sphere breasts of 850 ml each. More variability between the large phantom and small volunteer is seen in the g-factor averages/maximum values for the Sentinelle coil (see, e.g., rows 4 and 5 of Table 3).

Figure 7 displays an illustrative slice from data acquired in 3 volunteers. The first 2 rows display the fat suppressed 3D SPGR images using the 16 channel/31channel arrays. The images acquired with the two arrays are windowed and leveled in an identical manner. Note the better axilla coverage of the 31 channel array; in fact, for the last 2 volunteers, 3 outer-most coils were rendered inactive during the acquisitions for each side. For these relatively small/small-breasted subjects (bra size B and C), more than needed signal is arising from their backs. For the cases of large-breasted subjects, however, the outermost channels are only expected to reach into the axilla region. Rows 3 and 4 of Figure 7 display SNR maps acquired with the two coils, as described under Methods. The average SNR increase for the

3 volunteers achieved with the 31 channel array (computed over the breast area only) is 28%, ranging from 0% (volunteer 3) to 61% (volunteer 2). Accounting for the smaller g-factors of the 31 channel coil (Table 3), even higher SNR gains are expected for the 31 channel coils for accelerated scans. Note that the slices displayed for the 2 arrays represent the approximate center of the breasts, and do not perfectly match. Due to the flexible anatomy, and the significantly different support structure of the coils (with the sternum section being purposely widened for the 31 channel coil for increased comfort), perfect slice alignment can only be achieved with a good non-rigid registration software- unavailable to us.

Discussion and Conclusions

A novel, flexible, 31 channel, 3T breast coil was built; its performance was characterized and compared to the performance of the state-of-the art, 16 channel Sentinelle coil in a phantom and 3 normal volunteers. Limited dependence of the performance of our array on breast type and size was indicated by the network analyzer based phantom results of Table 2, and by the similarity of the noise correlation matrices between phantom and *in vivo* experiments of Figure 4. Higher (un-accelerated) SNR over the axilla area was demonstrated by our array both *in vitro* and *in vivo*-- requiring, in fact, turning off the 6 outermost array elements for small-breasted volunteers (Figure 7, volunteers 2 and 3). 68% higher unaccelerated SNR was observed over the breast area in a phantom (Figure 5). The same breast area exhibited un-accelerated SNR changes of 25%, 68% and 0% (averaging 28%) for the 3 volunteers studied (Figure 7) when the 31 channel coil was used. While this variability encountered *in vivo* is not consistent with the network analyzer measurements of Table 2, it is possible that our *in vitro* phantom setup (which contained a constant, relatively large “body”, coupled to various size spherical “breasts” of different compositions) did not accurately reflect the population seen in our small *in vivo* study. In fact, all our 3 volunteers weighed under 160 lbs, and were scanned with a 36–38 cm FOV; the torso phantom required a 48 cm FOV. Further studies documenting the performance of this coil in a large population are currently under way at University of Texas Southwestern (UTSW) Medical Center.

Generally lower g-factors, and the capability of accelerating in two dimensions were demonstrated for the 31 channel coil (Figure 6 and Table 3). Although arguably a good fraction of the acquisition protocols used for breast imaging only require L/R acceleration (as the phase encode direction is typically chosen in this direction, to minimize heart/respiratory motion induced artifacts), the capability of accelerating in all directions is important. For example, it may be preferable to choose the phase encode in the A/P direction in diffusion weighted imaging scans, so that the EPI ghosts do not overlap breasts. Multi-band excitations, on the horizon for improving the SNR of 2D acquisitions, would also benefit from the excellent acceleration capabilities of the 31 channel array.

While the initial building, tuning and matching of the coil was somewhat straightforward, its blocking was not trivial. In the absence of RF cables (while using only the cross-diodes of Figure 2 as passive blocking circuits), the array was very well blocked, and did not disturb the transmit field. Once the ~45 cm long RF cables, carrying the signal to the preamplifier

boards located in the abdominal area, were added to the array, significant (undesired) currents started flowing through the cables/array. Progressively stronger disturbance of the transmit field was seen towards the inferior side of the array, where many more cables were coming together (Figure 1c). This was mitigated, to a large extent, by ensuring that cables were routed through the midplane of the coils, adding 1 or 2 cable traps to each RF cable, and periodically joining the cable shields. Optical signal extraction would dramatically simplify the blocking of such complex arrays.

In our design, we have chosen to keep the preamplifiers off the coils, in a small enclosure in the coil housing, located near the subjects' abdominal region. While positioning the preamplifiers directly on the coil would have helped with coil decoupling, and allowed for much thinner outgoing cables, the SNR advantage of such an approach is questionable (15). More importantly, the addition of such fragile parts in a bending area could have limited the flexibility of the array (as the preamps would have needed to be mechanically protected), increase the possible heating to the patient, and create additional mechanical/electrical failure modes. Mounting the preamplifiers a short distance from the coil mitigates these problems, with no significant caveat.

As patient comfort is often a significant problem for breast coils, the 31 channel coil was designed with the mechanical and electrical parts decoupled from each other. Should the initial patient exams indicate the need for changes in the patient support structure to improve comfort, such changes can be easily implemented without impacting the electrical components of the coil. Additionally, even though our array was not designed for biopsy compatibility, it allows for easy lateral access, when the coil flap is let down (Figure 1e). For such a biopsy exam, the flap could be wrapped on the outside of the coil instead of through the opening for imaging (Figure 1d); the Velcro strip tying the two flaps together could then be simply untied for biopsying (Figure 1e). For frontal or medial biopsy access, however, a redesign of the mechanical support structure of the coil would be needed. A sparser main support structure (pink structure in Figure 1b), similar to the one of the Sentinelle coil, can allow for easy frontal access; an adjustable sternum support structure (mustard color in Figure 1b) can allow for medial needle access, while imaging would be performed with the coils on the (lifted) relevant flap. While such design modifications could be undertaken in the near future, the utility/advantage of the coil in clinical studies needs to be first demonstrated; the coil is currently in clinical use at UTSW Medical Center for this purpose.

Acknowledgement

The authors would like to acknowledge kind support and useful advice from Drs. Fraser Robb, Chris Hardy and Peter Roemer regarding coil blocking and decoupling.

Grant support: NIH 1R01CA154433

References

1. Kuhl CK. Current status of breast MR imaging. Part 2. Clinical applications. Radiology. 2007; 244(3):672–691. [PubMed: 17709824]
2. Sardanelli F. Overview of the role of pre-operative breast MRI in the absence of evidence on patient outcomes. Breast. 19(1):3–6. [PubMed: 20159456]

3. McLaughlin R, Hylton N. MRI in breast cancer therapy monitoring. NMR Biomed. 24(6):712–720. [PubMed: 21692116]

4. Jansen SA, Fan X, Medved M, Abe H, Shimauchi A, Yang C, Zamora M, Foxley S, Olopade OI, Karczmar GS, Newstead GM. Characterizing early contrast uptake of ductal carcinoma in situ with high temporal resolution dynamic contrast-enhanced MRI of the breast: a pilot study. Phys Med Biol. 55(19):N473–N485. [PubMed: 20858914]

5. Holdsworth SJ, Skare S, Newbould RD, Bammer R. Robust GRAPPA-accelerated diffusion-weighted readout-segmented (RS)-EPI. Magn Reson Med. 2009; 62(6):1629–1640. [PubMed: 19859974]

6. McGhee D, Steele J. Breast volume and bra size. Int J Clothing Sci and Technol. 2011; 23(5):351–360.

7. Nnewihe AN, Grafendorfer T, Daniel BL, Calderon P, Alley MT, Robb F, Hargreaves BA. Custom-fitted 16-channel bilateral breast coil for bidirectional parallel imaging. Magn Reson Med. 66(1): 281–289. [PubMed: 21287593]

8. Ouwerkerk R, Jacobs MA, Macura KJ, Wolff AC, Stearns V, Mezban SD, Khouri NF, Bluemke DA, Bottomley PA. Elevated tissue sodium concentration in malignant breast lesions detected with non-invasive 23Na MRI. Breast Cancer Res Treat. 2007; 106(2):151–160. [PubMed: 17260093]

9. Pruessmann KP, Weiger M, Scheidegger MB, Boesiger P. SENSE: sensitivity encoding for fast MRI. Magn Reson Med. 1999; 42(5):952–962. [PubMed: 10542355]

10. Roemer PB, Edelstein WA, Hayes CE, Souza SP, Mueller OM. The NMR phased array. Magn Reson Med. 1990; 16(2):192–225. [PubMed: 2266841]

11. Sacolick LI, Wiesinger F, Hancu I, Vogel MW. B1 mapping by Bloch-Siegert shift. Magn Reson Med. 63(5):1315–1322. [PubMed: 20432302]

12. Ohliger MA, Sodickson DK. An introduction to coil array design for parallel MRI. NMR Biomed. 2006; 19(3):300–315. [PubMed: 16705631]

13. Vaughn T, Griffiths J. RF coil for MRI. 2012 Sons Wa, editor.

14. Wiggins GC, Polimeni JR, Potthast A, Schmitt M, Alagappan V, Wald LL. 96-Channel receive-only head coil for 3 Tesla: design optimization and evaluation. Magn Reson Med. 2009; 62(3): 754–762. [PubMed: 19623621]

15. Hardy CJ, Giaquinto RO, Piel JE, Rohling KW, Marinelli L, Blezek DJ, Fiveland EW, Darrow RD, Foo TK. 128-channel body MRI with a flexible high-density receiver-coil array. J Magn Reson Imaging. 2008; 28(5):1219–1225. [PubMed: 18972330]

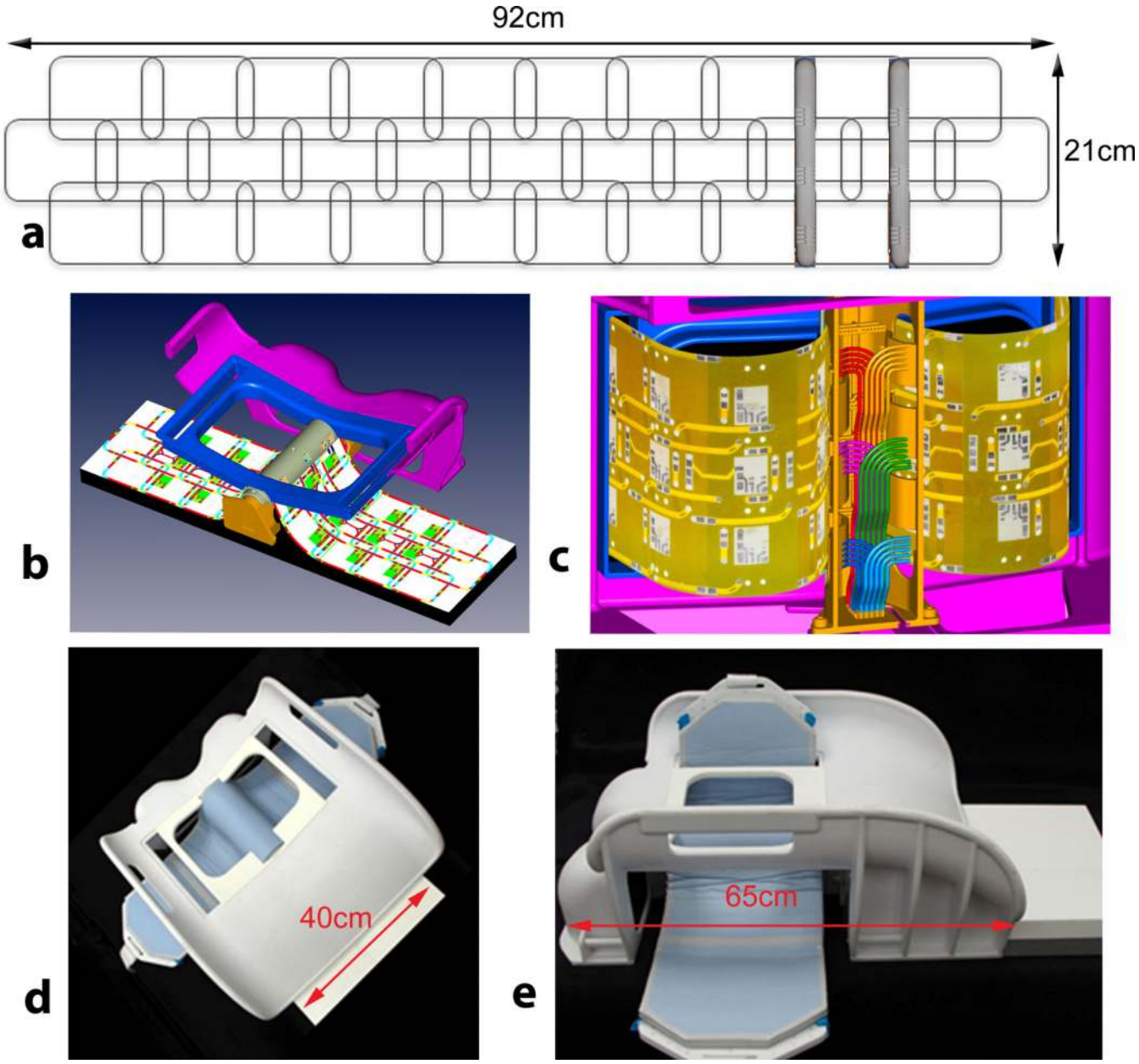

Figure 1.
31 channel coil images and illustrations: **a)** electrical layout **b)** cutout **c)** view from underneath **d)** top view **e)** lateral view

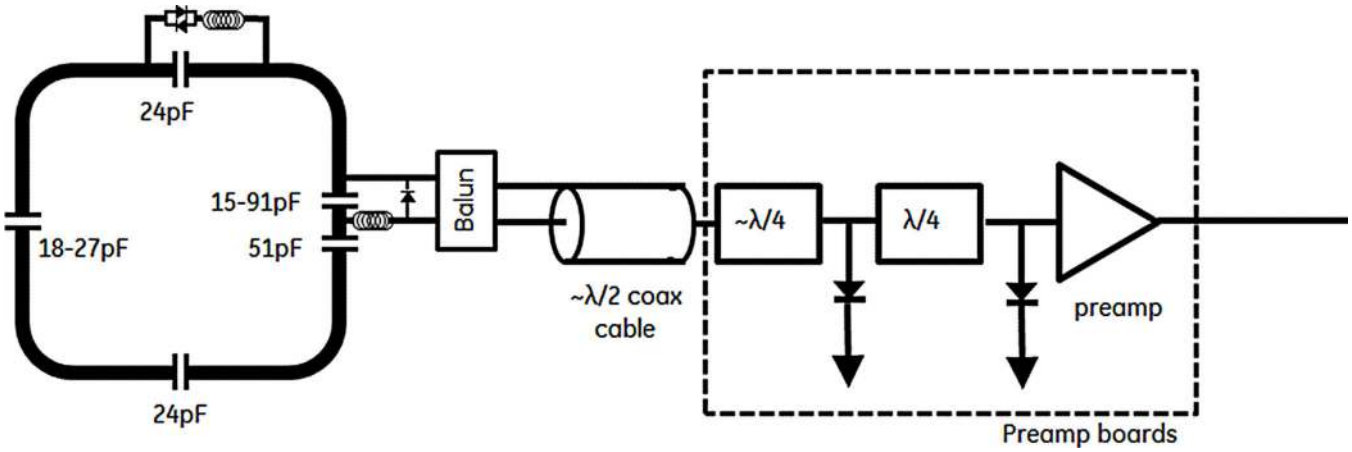

Figure 2.
Schematic of the circuit of each coil

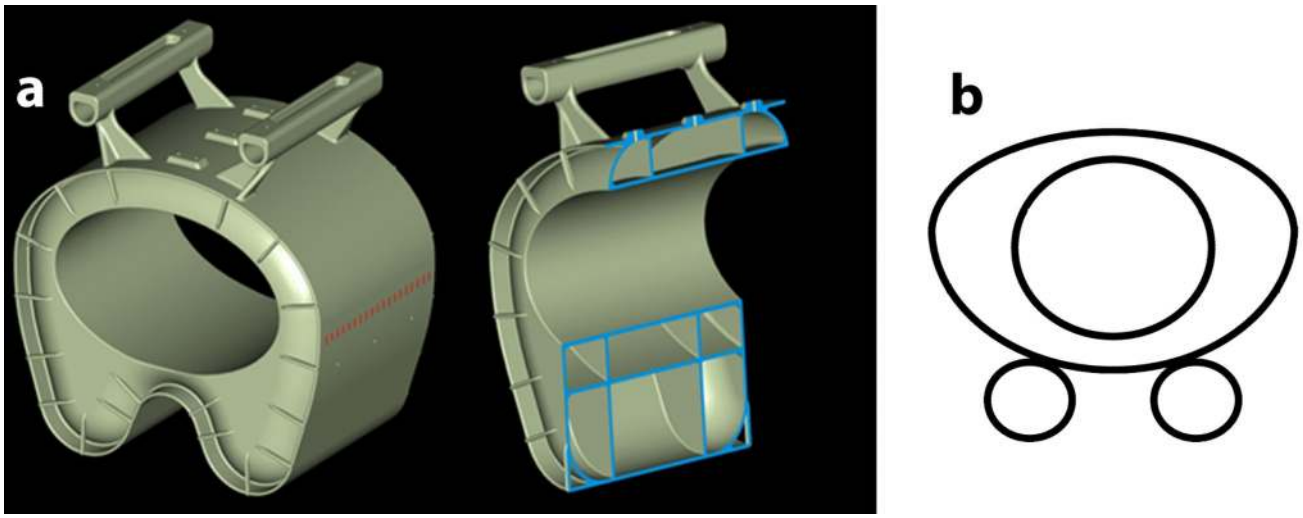

Figure 3.
Illustrations of the phantoms used for **a)** tuning the coil array **b)** verifying the sensitivity of coil tuning to different breast sizes and compositions.

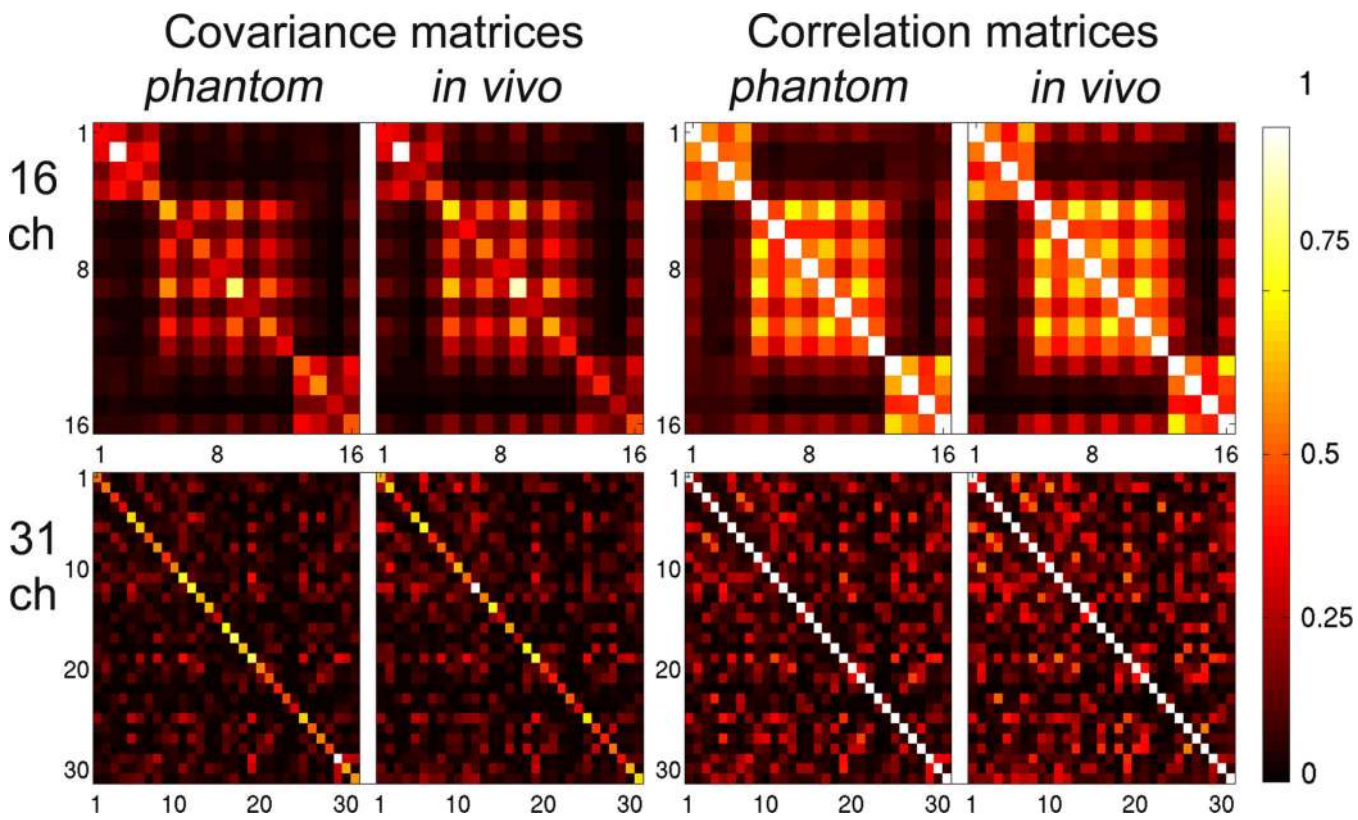

Figure 4.

The receiver noise covariance matrix (left) and its normalized version (correlation matrix) (right) for the 16 channel (top) and the 31 channel arrays (bottom), using a “hot” color map. The noise characteristics for both the phantom setup and one of the volunteers are shown in this figure.

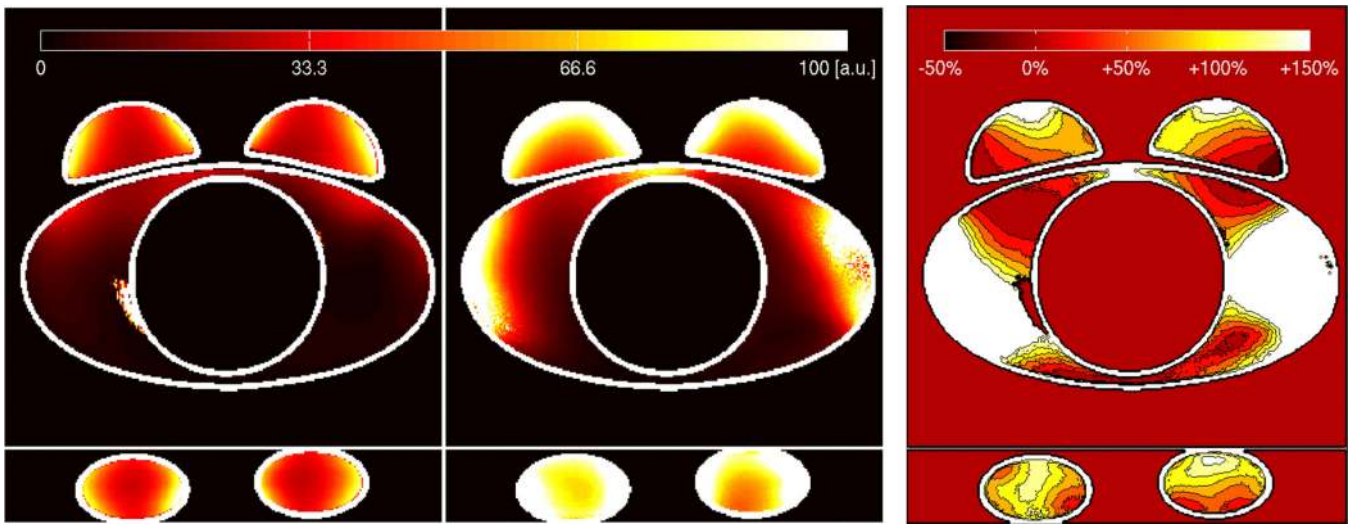

Figure 5.

SNR maps along axial (top) and middle coronal (bottom) orientations for the 16ch Sentinelle (left) and the 31ch (middle) coil using a "hot" color map. The figure on the right shows the relative percentage SNR improvement of the 31ch coil (relative to the 16ch one) in the form of a contour plot. The phantom outline is highlighted in white color.

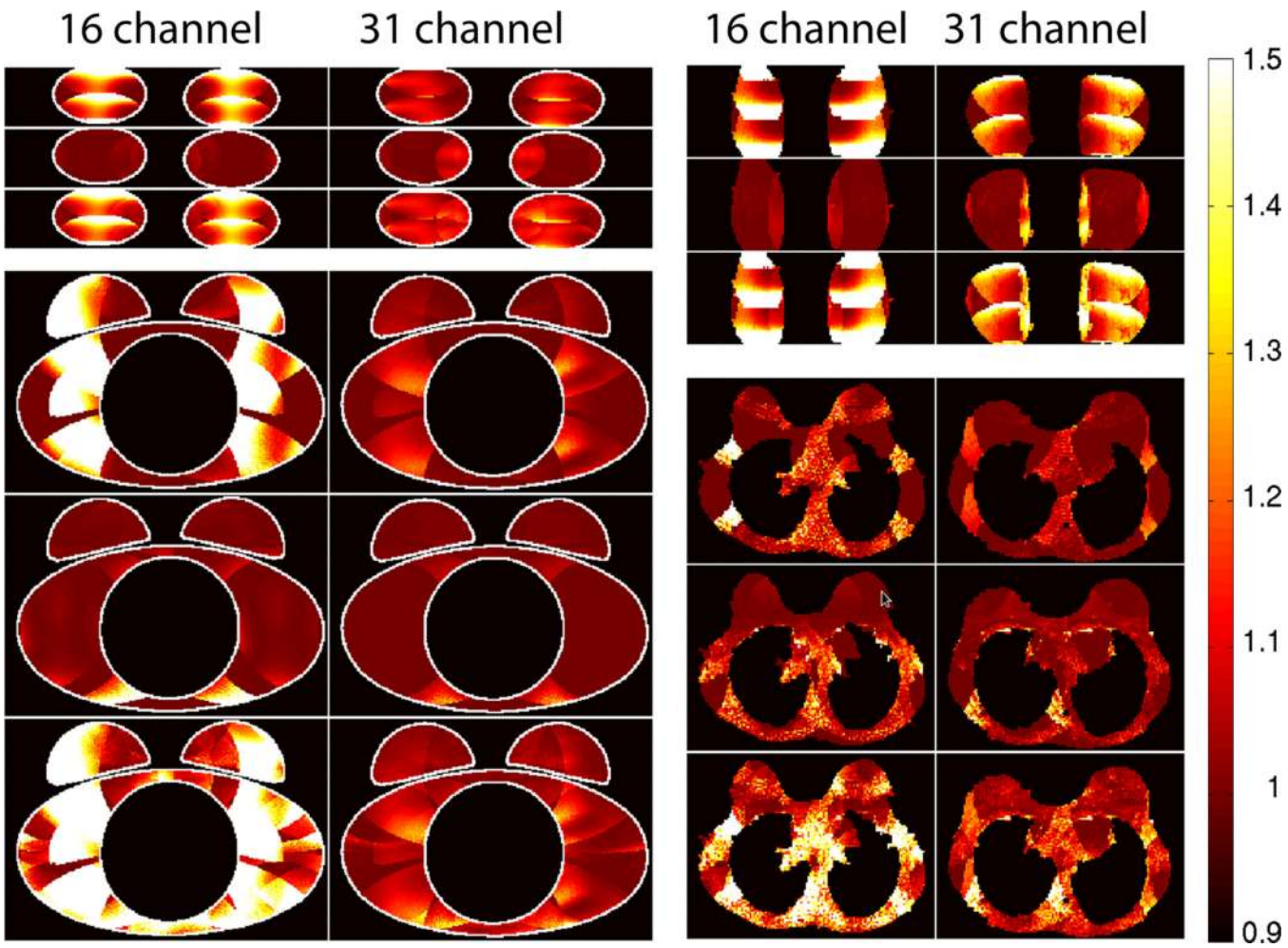

Figure 6.

Parallel imaging performance in terms of the g-factors for the 16 and 31 channel arrays, *in vitro* (left) and *in vivo* (right). The data was acquired fully sampled in a 3D acquisition, then undersampled for reconstruction. The top three rows show a coronal slice for acceleration factors of 1x2.4, 4.3x1, and 4.3x2.4.; the bottom three rows show an axial slice for acceleration factors of 1x2.8, 3x1, and 3x2.8. The direction of acceleration and acceleration factors used for this figure are identical to those in Table 3.

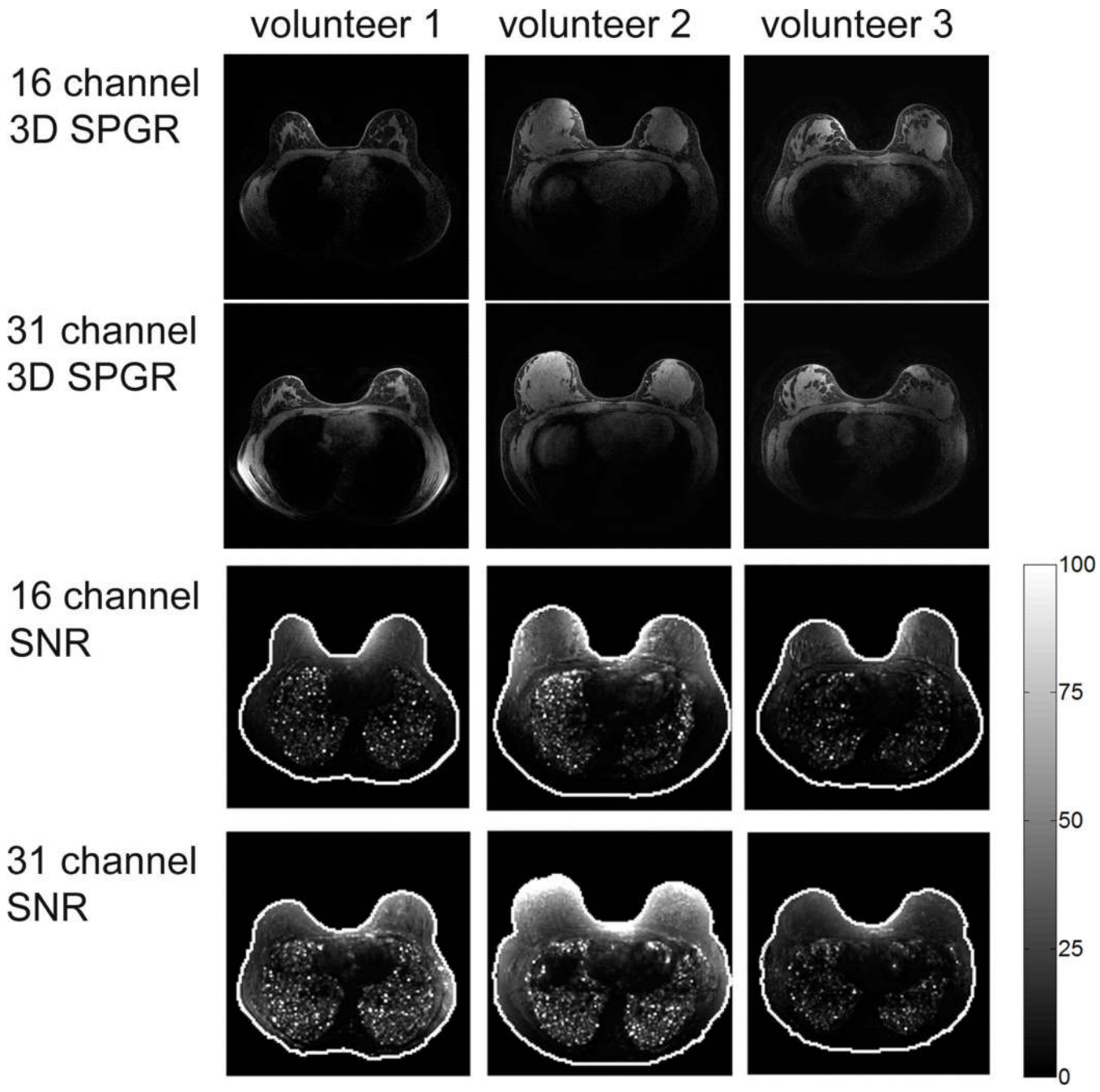

Figure 7.

Fat suppressed 3D SPGR images in 3 volunteers, acquired using the 16 channel Sentinelle coil (first row) and 31 channel coil (second row). The window and level for the two sets of images were identical. SNR maps in the same 3 volunteers, acquired using the 16 channel (third row) and 31 channel array (fourth row). The maps are also presented on the same scale for the 2 arrays.

Table 1

S11 and S21 parameters (in dB) for the 3 rows of the array elements

	S11 [dB]			S21 [dB]		
Array Row	**Minimum**	**Average**	**Maximum**	**Minimum**	**Average**	**Maximum**
Superior	−28	−19.2	−9.0	−51.1	−32.3	−20.7
Central	−30	−21.3	−16.0	−54.1	−33.6	−21.2
Inferior	−33	−20.9	−13.0	−51.3	−32.4	−19.4

Table 2

S11 parameters (in dB) for the 5 coils on the central row, from the center section (Ch1) to the outermost right coil (Ch5) as a function of loading

Phantom Size	NaCl concentration	S11 [dB] Ch1	S11 [dB] Ch2	S11 [dB] Ch3	S11 [dB] Ch4	S11 [dB] Ch5
Small	0	19	15	14	9	13
Small	1.1g/L	18	17	14	10	12
Small	2.2g/L	19	17	14	10	13
Medium	0	20	27	14	8	13
Medium	1.1g/L	20	27	14	9	13
Medium	2.2g/L	20	24	14	8	11
Large	0	16	16	12	17	7
Large	1.1g/L	16	14	13	13	11
Large	2.2g/L	17	13	12	12	6

Table 3

g-factor statistics for the two coils studied, for various acceleration factors. The data was acquired either in the phantom of Figure 5, or in a normal volunteer. The *in vivo* case is displayed in parantheses, underlined.

		Sentinelle		**31 channel**	
Orientation	**Acceleration**	**Average** ***in vitro*** ***(in vivo)***	**Maximum** ***in vitro*** ***(in vivo)***	**Average** ***in vitro*** ***(in vivo)***	**Maximum** ***in vitro*** ***(in vivo)***
Coronal	L/R × S/I = 1.0 × 2.4	1.65 (2.60)	13.46 (15.03)	1.07 (1.21)	1.43 (2.78)
Coronal	L/R × S/I = 4.3 × 1.0	1.01 (1.01)	1.07 (1.14)	1.02 (1.04)	1.16 (1.55)
Coronal	L/R × S/I = 4.3 × 2.4	1.68 (2.75)	13.86 (15.70)	1.10 (1.28)	1.51 (2.90)
Axial	L/R × A/P = 1.0 × 2.8	1.35 (1.04)	2.8 (1.68)	1.04 (1.05)	1.35 (1.68)
Axial	L/R × A/P = 3.0 × 1.0	1.07 (1.01)	1.96 (1.05)	1.01 (1.02)	1.37 (1.17)
Axial	L/R × A/P = 3.0 × 2.8	1.54 (1.12)	4.6 (2.32)	1.06 (1.05)	1.57 (1.43)